Precise branching ratio measurements in ^{19}Ne β decay and fundamental tests of the weak interaction

B. M. Rebeiro,[1] S. Triambak,[1,*] P. Z. Mabika,[1,2] P. Finlay,[3] C. S. Sumithrarachchi,[3,†] G. Hackman,[4] G. C. Ball,[4] P. E. Garrett,[3] C. E. Svensson,[3] D. S. Cross,[5] R. Dunlop,[3] A. B. Garnsworthy,[4] R. Kshetri,[4,5,‡] J. N. Orce,[1] M. R. Pearson,[4] E. R. Tardiff,[4,§] H. Al-Falou,[4] R. A. E. Austin,[6] R. Churchman,[4,‖] M. K. Djongolov,[4] R. D'Entremont,[6] C. Kierans,[7] L. Milovanovic,[8] S. O'Hagan,[9] S. Reeve,[6] S. K. L. Sjue,[4,¶] S. J. Williams,[4] and S. S. Ntshangase[2]

[1]*Department of Physics and Astronomy, University of the Western Cape, P/B X17, Bellville 7535, South Africa*
[2]*Department of Physics, University of Zululand, Private Bag X1001, KwaDlangezwa 3886, South Africa*
[3]*Department of Physics, University of Guelph, Guelph, Ontario N1G 2W1, Canada*
[4]*TRIUMF, 4004 Wesbrook Mall, Vancouver, British Columbia V6T 2A3, Canada*
[5]*Department of Chemistry, Simon Fraser University, Burnaby, British Columbia V5A 1S6, Canada*
[6]*Department of Astronomy & Physics, Saint Mary's University, Halifax, Nova Scotia B3H 3C3, Canada*
[7]*Physics Department, Simon Fraser University, Burnaby, British Columbia V5A 1S6, Canada*
[8]*Department of Physics & Astronomy, University of British Columbia, Vancouver, British Columbia V6T 1Z4, Canada*
[9]*Department of Science, University of Alberta Augustana Campus, Camrose, Alberta T4V 2R3, Canada*

(Received 4 October 2018; published 12 June 2019)

We used the 8π γ-ray spectrometer at the TRIUMF-ISAC radioactive ion beam facility to obtain high-precision branching ratios for ^{19}Ne β^+ decay to excited states in ^{19}F. Together with other previous work, our measurements determine the superallowed $1/2^+ \rightarrow 1/2^+$ β branch to the ground state in ^{19}F to be 99.9878(7)%, which is three times more precise than known previously. The implications of these measurements for testing a variety of weak interaction symmetries are discussed briefly.

DOI: 10.1103/PhysRevC.99.065502

I. INTRODUCTION

High-precision measurements of observables in ^{19}Ne β^+ decay offer several opportunities to rigorously test symmetries of the weak interaction. For example, correlation measurements from the decay have been used previously to search for second-class [1] and right-handed weak interactions [2,3], as well as set stringent limits on Fierz interference terms [4] and time-reversal-odd currents [5,6]. Such experiments have constituted valuable probes for physics beyond the standard model (BSM). In addition, precision measurements of ^{19}Ne β^+-decay transition probabilities provide a test of the conserved vector current (CVC) hypothesis, allowing a determination of V_{ud}, the up-down element of the Cabibbo-Kobayashi-Maskawa (CKM) quark mixing matrix [7], and are also important to test shell-model calculations [8,9] used to interpret parity mixing in ^{19}F [10,11].

In this paper, we report precise measurements of ^{19}Ne β^+-decay branches to excited states in ^{19}F, shown in Fig. 1. We briefly discuss the implications of our results for fundamental tests of the weak interaction.

II. EXPERIMENTAL DETAILS

A. Apparatus

The experiment was carried out using a radioactive ^{19}Ne ion beam ($T_{1/2} \approx 17.2$ s) at the TRIUMF Isotope Separator and Accelerator (ISAC) facility located in Vancouver, Canada. The beam was produced by bombarding a thick, heated SiC target with $\sim$20 μA of 500-MeV protons from the TRIUMF main cyclotron inducing spallation reactions. The diffused reaction products from the target were then introduced into a forced electron beam-induced arc-discharge (FEBIAD) ion-source via effusion. Subsequently, a pulsed mass-separated beam of $\sim 5 \times 10^5$ ^{19}Ne ions s^{-1}, with an energy of $\sim$37 keV was delivered to the 8π γ-ray spectrometer [12,13]. As shown schematically in Fig. 2, the spectrometer comprised an array of 20 symmetrically placed Compton-suppressed high-purity germanium (HPGe) detectors, whose inner volume consisted of 20 similarly placed 1.6-mm-thick BC404 plastic scintillator detectors called Scintillating Electron Positron Tagging Array (SCEPTAR) [12,13]. The SCEPTAR detectors were coupled to Hamamatsu H3165-10 photomultiplier tubes (PMTs) and covered $\sim$80% of the total solid angle. The radioactive ions were implanted on a $\sim$1.3-cm-wide, 40-μm-thick mylar-backed aluminum tape at the center of the 8π array. This tape

*striambak@uwc.ac.za
†Present address: National Superconducting Cyclotron Laboratory, Michigan State University, East Lansing, MI 48824, USA.
‡Present address: Department of Physics, The University of Burdwan, Burdwan 713104, West Bengal, India.
§Present address: Department of Physics and Astronomy, Northwestern University, Evanston, IL 60208, USA.
‖Deceased.
¶Present address: Physics Division, Los Alamos National Laboratory, Los Alamos, NM 87545, USA.

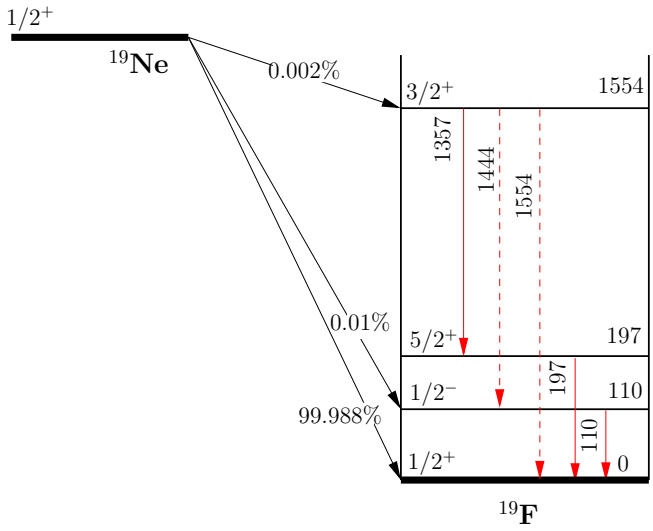

FIG. 1. Nominal decay scheme and γ transitions for ^{19}Ne β^+ decay. The decay proceeds predominantly via the superallowed $1/2^+ \rightarrow 1/2^+$ transition to the ground state in ^{19}F. The solid red lines represent the most intense γ transitions from excited states in ^{19}F. Level energies are in keV.

was part of a continuous moving tape collector (MTC) system that looped in vacuum through a lead-shielded aluminum box located downstream from the array center. The beam pulsing and the MTC allowed for data to be registered using tape cycles. In a typical cycle, the beam was implanted on the tape for a certain amount of time, following which the beam was "turned off" using an electrostatic deflector near the ion source. After a predetermined counting period, the MTC controls were triggered to move any potential long-lived activity on the tape away from the detectors into the shielded tape box.

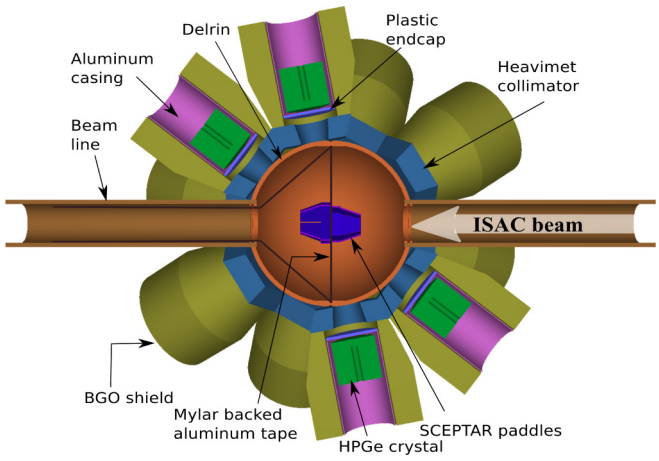

FIG. 2. Schematic picture of one hemisphere of the 8π array, shown together with the tape system. This model is drawn to scale and was used for the simulations described in the text.

B. Data acquisition

The data for this experiment were acquired with a fast encoding and read out ADC (FERA) system, with independent data streams for the SCEPTAR and HPGe detectors [13]. The data acquisition (DAQ) trigger included scaled β singles and β-γ coincidences for the scintillators and γ singles for the HPGe data stream. The events in each data stream were time-stamped using a LeCroy 2367 universal logic module (ULM) acting as a latching scaler, which counted pulses from a precision temperature-stabilized Stanford Research Systems 10 MHz $\pm$ 0.1-Hz oscillator.

The signals from the 20 SCEPTAR photomultiplier tubes were first shaped by a Phillips Scientific 776 fast amplifier and then sent in parallel to different parts of the data acquisition system. One output from each channel was sent to a LeCroy 4300 charge-to-digital converter (QDC) to generate the minimum ionizing β energy spectra. The other output was sent to an Ortec 935 constant fraction discriminator (CFD) for timing purposes. The 500-ns-wide pulses from the CFD were also sent in parallel to different units. One branch was converted to 50-ns-wide pulses using a fast Phillips Scientific 706 leading edge discriminator and sent to a logic OR fan-in-fan-out unit. The summed pulses from the individual SCEPTAR detectors were imposed with fixed nonextendible dead times in the range of 4–24 μs, much longer than any processing time in the preceding electronics. The dead-time-affected outputs were finally multiscaled using a Struck SIS3801 multichannel scaler (MCS). These MCS data were used to obtain a high-precision measurement of the ^{19}Ne half-life, which is described in Ref. [14]. The other branch was sent to multichannel CAEN 894 discriminators, from which the signals were fed to a 32-channel multihit LeCroy 3377 time-to-digital converter (TDC) to store β timing information.

The preamplifier output signals from the HPGe detectors were duplicated as well. The γ-ray energies were acquired using Ortec 572 spectroscopy amplifiers (with 3-μs shaping time) and Ortec AD114 peak sensing ADCs. In parallel, the preamplifier signals were sent to Ortec 474 timing filter amplifiers (TFAs) and subsequently discriminated using Ortec 583b CFDs. The fast output of the CFDs were further processed by the TDCs, providing timing information for the γ-ray events relative to the master trigger signal. These TDCs were additionally used to process the timing from the HPGe bismuth-germanate (BGO) Compton suppression shields, as well as the "inhibit" signals from the pulse pile-up rejection circuitry in the spectroscopy amplifiers.

Scaled-down β singles (with a scale-down factor of 255), γ singles and β-γ coincidence data were stored event-by-event in full list mode and reconstructed in an offline analysis.

III. ANALYSIS

A. Characteristics of the γ-ray spectrum

For this experiment the 8π MTC was configured [14] so that in each tape cycle we acquired background data for 2 s, following which the ^{19}Ne ions were collected for $\sim$1–2 s. A counting time of 300 s ($\sim$20 half-lives) was used to collect the decay data.

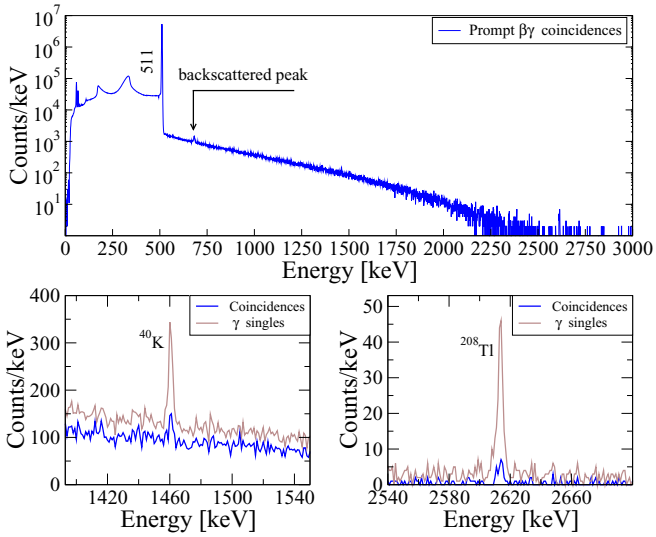

FIG. 3. Upper panel: γ-Ray spectrum for ^{19}Ne decay in coincidence with observed positrons. No beam contaminants are apparent from this spectrum, which expectedly is dominated by counts from 511-keV annihilation photons. The broad peak at approximately 680 keV arises from the backscatter of two simultaneous 511-keV γ rays. Lower panel: Overlay of γ-ray singles data with the coincidence spectrum. The data show that room background peaks were significantly reduced by gating on the prompt time differences between successive β and γ triggers registered with the ULM.

Figures 3 and 4 show the γ-ray spectrum obtained in coincidence with positrons registered with the SCEPTAR detectors. Similarly to other high-precision branching ratio measurements performed with the 8π array [15–17], this spectrum was obtained by gating on the time differences between successive β and γ triggers registered with the ULM. These data were acquired from the same cycle time window that used to determine the total observed β singles (which is described in Sec. III C). As further illustrated in Fig. 4, we clearly identify two γ-ray peaks at 110 and 1357 keV that arise from the 110 → 0- and 1554 → 197-keV transitions in the daughter ^{19}F nucleus. The γ-ray peak from the 197 → 0-keV transition is not visible because of the large Compton artefact in that region of the spectrum. We also do not observe explicit signatures of the (much weaker) 1554- and 1444-keV γ rays (cf. Fig. 1) in these data. However, this did not have

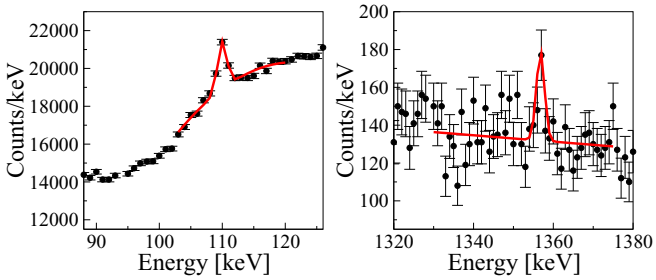

FIG. 4. Fits to the 110- and 1357-keV peaks in the coincident γ-ray spectrum. These peaks arise from the 110 → 0- and 1554 → 197-keV transitions shown in Fig. 1.

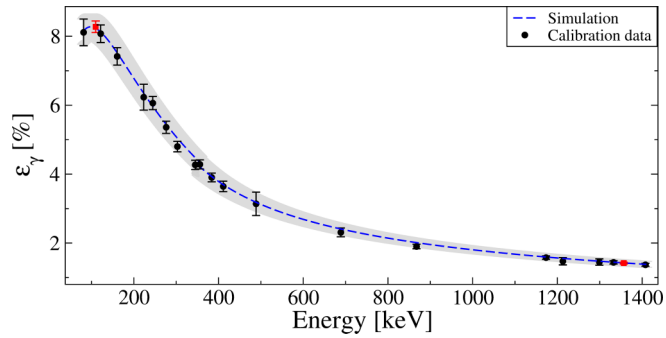

FIG. 5. Experimentally determined γ-ray efficiencies for the 8π array in the range $80 \leqslant E_\gamma \leqslant 1408$ keV. The dashed curve outlines normalized simulated efficiencies for individual γ rays determined using the PENELOPE code. The gray band represents our conservative estimate of the total uncertainty in the simulations. The red squares show the determined efficiencies at 110 and 1357 keV, respectively, that were eventually used to determine the branching ratios of interest.

a bearing in our determination of the β-decay branches, as discussed below.

B. Efficiency calibration

The HPGe detection efficiency for the array was determined using a combination of Monte Carlo simulations performed with the PENELOPE radiation transport code [18] and data obtained from standard ^{133}Ba, ^{152}Eu, and ^{60}Co sources. The absolute activities of the latter were known to 3% at the 99% CL.

The reasons for performing the simulations were twofold:

(1) To obtain coincidence summing corrections due to γ-ray cascades in the calibration sources.
(2) To offer a comparison between the simulated efficiencies and the experimentally determined values.

Figure 5 shows the extracted efficiencies for the calibration γ rays after applying small corrections due to both coincidence summing as well as pulse pile-up.[1] These values are found to be in excellent agreement with the results from the PENELOPE simulations (for multiplicity 1 photons), apart from an overall normalization factor.

Once we ascertained the credibility of the PENELOPE model, the simulations were used both to determine γ-ray summing corrections for ^{19}Ne β decay (described in Sec. IV) and the attenuation of photons due to absorption in the tape material. Using a ^{19}Ne implantation profile from TRIM [19,20],[2] the simulations showed that the attenuation was

[1]The summing corrections were of the order $\lesssim$2%, while the pile-up corrections were of the order $\lesssim$0.3%. Incorporating known γ-γ angular correlations in the simulations had an insignificant effect on the former.

[2]The ^{19}Ne source was assumed to be uniformly distributed on the tape over a 3 mm radial diameter. TRIM predicts a nearly Gaussian implantation (depth) profile, with a range of ∼700 Å and straggle

negligible for the 1357-keV γ ray, whose efficiency was eventually determined from a polynomial fit to the calibration points

$$\ln \epsilon_\gamma(i) = \sum_{j=0}^{3} a_j \, [\ln E_\gamma(i)]^j. \quad (1)$$

On the other hand, the efficiency for the 110-keV γ ray needed a small correction ($\sim$1.5%) to the value determined from the above equation, due to γ-ray absoprtion within the tape. Our extracted efficiencies for both the γ rays are highlighted in red in Fig. 5.

C. β singles determination

Similarly as described in Ref. [21], we obtained absolute β-decay branches to the excited $1/2^-$ and $3/2^+$ states in ^{19}F from the ratios of β-γ coincident counts to the total number of observed β singles. Hence, an important step in our analysis was to obtain the integrated number of β singles events (N_β) detected by the SCEPTAR array. This was determined by a maximum likelihood fit to the total β activity (sum of the scaled-up β singles and the γ coincident β-decay curves) assuming Poisson-distributed statistics [22]. The fitted number of counts in each time bin (of width t_b) was described by the function

$$y_{\rm fit}(i) = \frac{y(i)}{\left[1 + \frac{y(i)}{N_c t_b}\tau_{\rm eff}\right]}, \quad (2)$$

where

$$y(i) = \int_{t_l}^{t_h} A_1 \exp\left(\frac{-\ln 2}{T_{1/2}} t\right) dt + \int_{t_l}^{t_h} A_2 \, dt. \quad (3)$$

Equation (2) represents a realistic model for N_c cycles of data that are affected by an instrumentation dead time $\tau_{\rm eff}$ per β event. Figure 6 shows the summed β activity curve generated from the list-mode ULM data for a total of 724 cycles recorded over the course of our experiment. These data were fitted using fixed values[3] of $T_{1/2}$ and $\tau_{\rm eff}$, while the A_1 and A_2 parameters were varied as free parameters. Since the data were the sum of several experimental runs with different implant times, we circumspectly chose the range of the fit to be from $t = 6$ s to $t = 200$ s. This time interval corresponds to approximately 11 half-lives. While it is large enough to provide a reasonably accurate understanding of the background, it avoids the $t > 10T_{1/2}$ region where the ^{19}Ne activity does not play a statistically significant role.

The optimal value of $\tau_{\rm eff}$ was determined from an algorithm that performed the fits described above over a large range of dead times $1.5\,\mu{\rm s} \leqslant \tau_{\rm eff} \leqslant 4.5\,\mu{\rm s}$, in steps of $\Delta\tau_{\rm eff} = 10^{-4}\,\mu$s. The $\tau_{\rm eff}$ corresponding to the minimum χ^2 ($\tau_{\rm eff} = 3.5\,\mu$s) was eventually used to obtain the total number of β singles recorded.

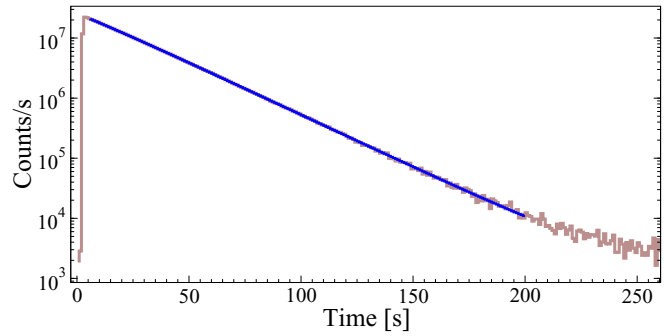

FIG. 6. Best fit to the dead-time-affected β singles activity curve. The total χ^2 for the fit is 30 627 for 193 degrees of freedom, which is rather poor. However, this has an inconsequential effect on the eventual determination of β-decay branches. The data described in this analysis were restricted to those runs that were collected at initial β rates of $\lesssim$1 kHz per paddle [14]. In comparison, the measured γ-ray rates averaged approximately 150 Hz over the whole experiment.

The best fit to our data on using the optimal value for the effective dead time is shown in Fig. 6. The reduced $\chi^2_{\rm min}$ value for this highly constrained fit is rather poor, but not unexpected, considering the high statistics acquired. More realistically, to obtain an improved fit to the data, one would require the incorporation of rate-dependent effects and an accurate understanding of additional complications such as scintillator afterpulsing [14]. To bypass this problem we choose to make an overly conservative estimation of the total uncertainty on the extracted N_β value. This was done by using a 99.9% confidence level uncertainty on $\tau_{\rm eff}$ and further inflating the uncertainty in A_1 by a scale factor of $\sqrt{\chi^2/\nu}$ for ν degrees of freedom. Both these uncertainties were added in quadrature to the uncertainty contribution from the half-life value. This procedure yielded a final value of $N_\beta = 5.655(3) \times 10^8$ registered in the time range of the fit.

Although the γ-ray spectrum in Fig. 3, and the half-life analysis described in Ref. [14] show no obvious indication of contaminants in the beam, a small contamination of molecular ^{18}F^{1}H cannot be ruled out. However any such contamination would not consequentially affect our measurements, mainly because the long half-life of ^{18}F ($T_{1/2} \approx 110$ min) would result in an almost constant decay rate over 300 s. Furthermore, the decay of ^{18}F does not feed any excited levels in ^{18}O. Therefore its presence in the beam would only result in an increased background component A_2 and not affect our β singles determination described above.

IV. RESULTS

If one neglects the small electron-capture fraction for the β decay, then the ratio of the number of β-γ coincidences for a given γ transition from level $i \rightarrow j$ to the *total* number of N_β

of $\sim$290 Å. The final uncertainties in the extracted efficiencies also included the effect of a (conservative) 1 mm offset in the beam spot laterally.

[3]The ^{19}Ne half-life used for the fit was from a weighted mean of the results from three recent high-precision measurements [14,23,24]. We refrain from using the result of Broussard *et. al.* [25] due to the inconsistency of their measurement with the other three highest-precision results [24].

TABLE I. Relative uncertainties contributing to the first forbidden branch in ^{19}Ne β^+ decay.

Source	Correction	$\frac{\Delta B_1}{B_1}$ (%)
Coincidence summing	1.0089(6)	0.06
Random coincidences	0.961(9)	0.94
Pile up	1.00324(1)	0.001
Dead time	1.00577(6)	0.006
Q_β value dependence on β efficiency	1.000(2)	0.20
$N_{10}^{\beta\gamma}/N_\beta$ ratio		6.4
HPGe efficiency (ϵ_{10})		2.4

singles is simply

$$\frac{N_{ij}^{\beta\gamma}}{N_\beta} = \frac{1}{\sum_m B_m\eta_m}\left[B_i\eta_i + \sum_{k>i} B_k\eta_k\gamma_{ki}\right]\gamma_{ij}\epsilon_{ij}, \quad (4)$$

where B_i is the β branch to the ith level, η_i is the β detection efficiency for β-decays feeding level i, γ_{ij} is the probability of a γ transition from level i to j, and ϵ_{ij} is the efficiency of detecting that γ ray. This expression can be simplified further to obtain the β branches in Fig. 1. For example, we determine B_1 using the photopeak area of the 110-keV γ ray and the simple expression

$$B_1 \simeq k_1\left(\frac{N_{10}^{\beta\gamma}}{N_\beta\epsilon_{10}}\right), \quad (5)$$

which neglects the contribution with the vanishingly small product $B_3\gamma_{31}\epsilon_{10}$. The B_3 branch was obtained similarly. For both these cases, the $N^{\beta\gamma}$ were extracted from a γ-ray spectrum (shown in Figs. 3 and 4) that was projected out from the same cycle time window that was used to determine the total number of β singles.

In the above, k_1 is a correction factor ($\sim$1) which accounts for small systematic effects and is imperative for an accurate result. Analogous to the approach followed in Ref. [21], we determined this factor[4] from the product of five distinct corrections that are listed in Table I and described below.

A. Summing corrections (k_s) and random coincidences (k_r)

The γ-ray spectrum in Fig. 3 does not show an explicit signature of photopeak summing with 511-keV annihilation photons, due to the large continuum in the region around 621 keV. Nevertheless, it was important to estimate the photopeak summing with 511-keV γ rays, in addition to other summing contributions from scattered positrons, bremsstrahlung, and Compton-scattered radiation. Therefore an important part of our analysis was to estimate the coincidence summing corrections k_s for the two γ rays of interest. We quantified these corrections with additional PENELOPE Monte Carlo simulations that tracked both the positrons and the photons in the active volume of the array, while also taking into account positron annihilation in flight.

[4]Similarly, a correction factor k_3 is used to determine B_3.

TABLE II. A comparison of branching fractions obtained from this measurement to previous work.

Transition	Measured β branch (%)		
	Previous work		This work
$1/2^+ \rightarrow 3/2^+$	0.0021(3)[a]	0.0023(3)[b]	0.0017(5)
$1/2^+ \rightarrow 1/2^-$	0.012(2)[c]	0.011(9)[d]	0.0099(7)

[a]D. E. Alburger [30].
[b]E. G. Adelberger *et al.* [10].
[c]E. G. Adelberger *et al.* [31].
[d]E. R. J. Saettler *et al.* [32].

Our simulations show that roughly 0.9% of the 110-keV γ rays were lost due to coincidence summing. In comparison, the correction for the 1357-keV peak was $k_s = 1.0119(5)$. This value is slightly larger than that for the 110-keV γ-ray due to an additional contribution from the 1357 $\rightarrow$ 197 $\rightarrow$ 0-keV cascade, which is significant and therefore cannot be ignored.

On the other hand, we determine the correction factor for random β-γ coincidences to be $k_r = 0.961(9)$. This was obtained from the intensity ratios of the background γ-ray lines observed in the prompt-coincidence and singles γ-ray spectra (shown in the lower panels of Fig. 3) together with the known absolute efficiency of the SCEPTAR array.

B. Dead time (k_d) and pile up (k_p)

The latching scalers in the ULM enabled HPGe and SCEPTAR dead times to be calculated independently on an event-by-event basis [26]. While the SCEPTAR dead time effectively cancels out in Eq. (4), the γ-ray photopeak areas required an additional dead time correction. The average dead time per event for the HPGe data stream was found to be 30.4(3) μs. Using this value we obtain a HPGe dead time correction factor $k_d = 1.00577(6)$. Independently, we also obtain a pile-up correction $k_p = 1.00324(1)$ from the events registered by the pile-up TDC that were vetoed from the final γ-ray spectrum.

C. β Endpoint energy dependence on SCEPTAR efficiency (k_β)

This small correction factor is important for the B_3 branch, where the β energy distribution is very different than the ones feeding the ground and first excited states in ^{19}F. It is given by

$$k_{\beta 3} = \frac{1}{\eta_3}\sum_{m=0,1,3} B_m\eta_m. \quad (6)$$

We determined this correction from simulations of SCEPTAR efficiencies for the different Q_β values feeding the three states of interest at 0, 110, and 1554 keV. The simulations show that the B_3 branch requires a correction factor of $k_{\beta 3} = 1.044(2)$. Expectedly, this correction for the B_1 branch agrees with unity (as $\eta_0/\eta_1 \approx 1$). More detailed investigations of the Q_β value dependence on SCEPTAR efficiency can be found in Ref. [27].

Table II compares our results from this experiment with previous work. While in excellent agreement with earlier

measurements,[5] our result for the $1/2^+ \to 1/2^-$ first-forbidden branch is ≈2.4 times more precise than the previous highest-precision measurement. A weighted mean of the results yields final branching ratios of $B_1 = 0.0101(7)\%$ and $B_3 = 0.0021(2)\%$. This directly translates to a ground-state superallowed branch of 99.9878(7)%, which is three times more precise than the value reported in a previous compilation [29]. Since our published ^{19}Ne half-life result [14], there have been three additional half-life measurements reported with comparable or better precision. Similarly to our experiment, the authors of Refs. [23,24] used the method of β counting, while Broussard *et al.* [25] determined the half-life using 511-keV annihilation radiation detected in two collinear HPGe detectors. A weighted mean of the four values yields a poor χ^2 probability of $P(\chi^2, \nu) \approx 1\%$. This is not unexpected, since the γ-ray measurement disagrees with the other three measurements and is more than 3σ away than the latest (and most precise) value published in Ref. [24]. The probability improves to 65% if we exclude the value from Ref. [25]. Since this discrepancy is yet to be resolved, for our subsequent analysis we choose to use an average value of $T_{1/2} = 17.257(2)$ s, obtained using only the results from Refs. [14,23,24].[6]

Together with the electron-capture branching fraction [29,33,34], the mass excesses from the most recent Atomic Mass Data Center compilation [35,36] and other small corrections [29] due to isospin symmetry breaking and radiative effects, we obtain a corrected $f_V t$ value for the $1/2^+ \to 1/2^+$ ^{19}Ne superallowed β decay to be

$$\mathcal{F}t^{^{19}\mathrm{Ne}} = f_V t(1+\delta_R')\left(1+\delta_{\mathrm{NS}}^V - \delta_C^V\right) = 1721.44(92)\,\mathrm{s}, \tag{7}$$

where we follow the same notation as Refs. [29,37] and $f_V = 98.649(31)$ is the vector component of the statistical rate function for the transition.[7]

As a result of the aforementioned high-precision half-life and β branch measurements, the value in Eq. (7) is now one of the most precisely measured $\mathcal{F}t$ values for $T = 1/2 \to T = 1/2$ mirror transitions. Consequently, it provides a benchmark for comparison with experimental observables that are used for searches of BSM physics. We discuss some examples below.

V. DISCUSSION

A. Implications for searches of second-class weak interactions

Beyond the allowed approximation, the hadronic weak current contains additional *recoil-order* form factors [38,39,41,42]. Some of these terms are classified as *second class*, based on their transformation properties under the G-parity operation [38,43]. Within the limit of perfect isospin symmetry, second-class currents are forbidden in the standard model. Angular correlation measurements in nuclear β decays are known to be useful probes to search for induced second-class currents [41,44]. As an example, we focus on the β^+ decay of spin-polarized ^{19}Ne nuclei. After integrating over the neutrino directions, the differential decay rate can be expressed in terms of the spectral functions $f_i(E)$ [44],

$$d\Gamma \propto (E_0 - E)^2 pE\left\{f_1(E) + f_4(E)\frac{\langle \boldsymbol{J}\rangle}{J}\cdot\frac{\boldsymbol{p}}{E} + \cdots\right\} dE\, d\Omega_e, \tag{8}$$

where

$$f_1(E) = a^2 + c^2 - \frac{2E_0}{3M}(c^2 - bc - cd) + \frac{2E}{3M}(3a^2 + 5c^2 - 2bc) - \frac{m_e^2}{3ME}(2c^2 - 2bc - cd) \tag{9}$$

and

$$f_4(E) = \sqrt{\frac{J}{J+1}}\left[2ac - \frac{2E_0}{3M}(ac - ab - ad) + \frac{2E}{3M}(7ac - ab - ad)\right] + \left(\frac{1}{J+1}\right)\left[c^2 - \frac{2E_0}{3M}(c^2 - bc - cd) + \frac{E}{3M}(11c^2 - 5bc + cd)\right]. \tag{10}$$

In the above, $J = 1/2$, E is the total energy of the positrons, E_0 is the end-point energy, $\boldsymbol{p}$ is the positron momentum, m_e is the positron mass, and M is the average of the parent and daughter masses. The remaining terms are momentum-transfer dependent form factors; $a(q^2)$ and $c(q^2)$ are the leading vector and axial-vector form factors, $b(q^2)$ is the weak magnetism form factor, and $d(q^2)$ is an induced-tensor form factor. It is apparent from Eq. (8) that if one ignores small electromagnetic corrections due to final-state Coulomb interactions [45], then the β asymmetry parameter $A_\beta(E)$ for the decay can be defined in terms of these spectral functions, so that $A_\beta = f_4(E)/f_1(E)$.

In the low-momentum transfer ($q^2 \to 0$) limit, $a = C_V M_F$ and $c = C_A M_{\mathrm{GT}}$, where M_F and M_{GT} are the usual Fermi and Gamow-Teller matrix elements [29]. Both these and the other energy-dependent (recoil-order) terms in the spectral functions can be determined using the CVC hypothesis [46]. For ^{19}Ne β^+ decay, the vector and weak magnetism form factors reduce to $a = 1$ and $b = -148.5605(26)$ [7], where the latter is calculated from the magnetic moments of the parent and daughter nuclei [44]. The standard-model-allowed (first-class) contribution to the induced-tensor form factor is expected to be highly suppressed as the decay mainly occurs between isobaric analog states [44]. Finally, the standard

[5] We do not include the 1975 result of B_3 by Freedman *et al.* [28] as it significantly disagrees with all subsequent work, including ours.

[6] If we include the result from Ref. [25], the weighted mean changes insignificantly to $T_{1/2} = 17.258(2)$ s.

[7] This is slightly different than the axial-vector part, mainly because of the effect of weak magnetism [38,39] on the shape-correction factor of the latter [21]. We use $f_A/f_V = 1.0142(28)$ [40], where, similar to Ref. [7], we assign a 20% relative uncertainty on the deviation of f_A/f_V from unity.

TABLE III. Measured A_β values (in %) for ^{19}Ne superallowed decay. For comparison we list the standard model predictions obtained using the $\mathcal{F}t$ value in Eq. (7).

Year	Reference	$A_\beta(0)$[a]	A_β[b]
1963	Commins and Dobson [47]	–	−5.7(5)
1967	Calaprice *et al.* [48]	–	−3.3(2)
1969	Calaprice *et al.* [49]	–	−3.9(2)
1975	Calaprice *et al.* [1]	−3.91(14)	–
1983	Schreiber [50]	−3.603(83)	–
1996	Jones [51]	−3.52(11)	–

[a]Standard model prediction for $A_\beta(0) = -4.15(6)\%$.
[b]Standard model prediction for $A_\beta = -4.49(6)\%$.

model value for the Gamow-Teller form factor c can be extracted from the averaged $\mathcal{F}t$ value of $0^+ \to 0^+$ superallowed Fermi transitions [37] (or, equivalently, V_{ud}) and $\mathcal{F}t^{^{19}\mathrm{Ne}}$. We determine this to be $c_{\mathrm{SM}} = -1.5916(23)$.[8]

There have been several measurements of ^{19}Ne β^+-decay asymmetry performed in the past. These are listed in Table III. Furthermore, since the weak magnetism and induced-tensor form factors affect the energy dependence of A_β, a measurement of the slope dA_β/dE allows a sensitive search for second-class currents. This approach was first used by Calaprice *et al.* [1] to search for second-class currents in ^{19}Ne decay. Interestingly, their measurement significantly disagreed with CVC predictions, requiring an unexpectedly large second-class tensor form factor to describe the data. Calaprice *et al.* also reported a zero-kinetic-energy intercept value for the β asymmetry, which is listed as $A_\beta(0)$ in Table III. This work was followed by two other measurements whose results were never published but reported in Ph.D. theses [50,51]. Although the dA_β/dE results from the three experiments are in reasonable agreement with each other, the unpublished values are more consistent with the standard model prediction and other experimental results that do not show explicit signatures of second class currents [52–55].

For completeness we list these results together with earlier β asymmetry measurements in Tables III and IV. It is worthwhile to note that unlike Refs. [1,50,51], the older measurements [47–49] were performed by integrating over the whole positron spectrum.

If one assumes $d = 0$, then the measured A_β coefficient can be used to determine the axial-vector form factor for the decay, independent of other standard model expectations. This is shown in Fig. 7, where we plot the value for c extracted from all previous β asymmetry measurements[9] for ^{19}Ne decay. Clearly, these data are in conflict with the CVC prediction and with each other. Some consequences of these differences are discussed below.

[8]This form factor has a negative sign because we follow the same representation for Dirac matrices as Ref. [44]. Standard-model-allowed recoil-order corrections [41] are taken into consideration in this calculation and hereafter.

[9]For the $A_\beta(0)$ measurements $E = 0.511$ MeV. For the others we use an averaged value of $E = 1.474$ MeV for the positrons.

TABLE IV. Measured dA_β/E values for ^{19}Ne superallowed decay. Similarly as in Table III, the standard model prediction for the slope is listed for comparison.

Year	Reference	dA_β/dE[a] (% MeV^{-1})
1975	Calaprice *et al.* [1]	−0.65(15)
1983	Schreiber [50]	−0.486(77)
1996	Jones [51]	−0.42(11)

[a]$(dA_\beta/dE)_{\mathrm{SM}} = -0.349(2)\%\,\mathrm{MeV}^{-1}$.

B. Implications for searches of right-handed currents

Despite the observed V-A character of weak interactions, some of the earliest extensions to the standard model [56,57] and their more modern versions [58,59] use a parity-symmetric Lagrangian [60] to describe the theory. These models restore parity at a higher energy scale and provide a framework within which the apparent nonconservation of parity at lower energies can be attributed to the spontaneous breakdown of a higher gauge symmetry [59–61]. The extended gauge group requires the existence of additional right-handed W and Z bosons, which are much heavier than their left-handed counterparts.

Such models present a compelling case. Not only does the inherent left-right (LR) symmetry make them aesthetically pleasing, but also the suppression of $V + A$–type weak interactions at low energies is a natural consequence in these models, due to the large masses of the right-handed gauge bosons. It has also been shown that this suppression has a direct relation to both the smallness of neutrino masses [62] as well as the experimentally observed CP violation [63].

In the simplest (manifest) LR models [60], the left-handed and right-handed charged weak currents couple to the weak interaction eigenstates W_L and W_R and have identical transformation properties (apart from chirality).[10] On account of the symmetry breaking, the mass eigenstates are simply linear combinations of the weak interaction eigenstates, with a LR mixing angle ζ [60]. The weak interaction can therefore be parameterized [64] in terms of ζ and the ratio $\delta = (M_1/M_2)^2$, where M_1 (M_2) is the mass of the left- (right-) handed boson, with $M_1 \ll M_2$. Following Holstein and Treiman [3] and Bég *et al.* [60], one can further define two new parameters x and y, which are related to δ and ζ. For sufficiently small δ and ζ, these reduce to $x \simeq \delta - \zeta$ and $y \simeq \delta + \zeta$ [64]. Such a prescription ensures that purely left-handed weak interactions would emerge for vanishing values of x and y.

The above parametrization modifies the f_1 and f_4 spectral functions to allow for right-handed currents (RHCs), such

[10]Here, the left-handed and right-handed sectors have identical coupling constants and mixing angles. There are no additional CP violating phases apart from the usual Kobayashi-Maskawa phase [59].

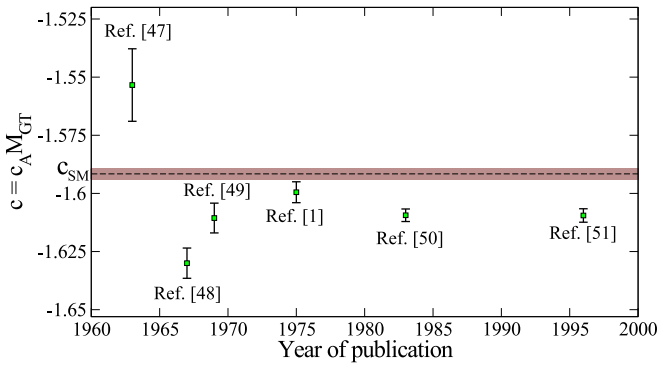

FIG. 7. The axial-vector form factor for ^{19}Ne β^+ decay obtained from independent β asymmetry measurements. The standard model prediction c_{SM} obtained from this work is shown for comparison.

that [3]

$$f_1 \to f_1 + x^2 a^2 + y^2 c^2, \tag{11}$$

$$f_4 \to f_4 - \frac{y^2 c^2}{J+1} - 2\sqrt{\frac{J}{J+1}}\, xyac. \tag{12}$$

This makes the experimentally measured A_β parameter sensitive to right-handed weak interactions.[11]

We have already shown in Table III that the β asymmetry for ^{19}Ne decay is quite small. This is due to an accidental cancellation of the leading form factors in Eq. (10). Evidently, a similar cancellation does not take place for the RHC contribution in Eq. (12), except when $x = y$. This makes ^{19}Ne β decay highly sensitive to RHCs. As a matter of fact, it is the most sensitive probe for RHCs among all mirror transitions up to $A = 41$ [65]. For example, using a "sensitivity coefficient" defined by the authors of Ref. [65], it is calculated to be $\sim$70 times more sensitive [65] than ^{37}K β decay, whose β asymmetry was recently reported [66] with the highest relative precision among all $T = 1/2$ nuclides.

Unless the ratio of axial-vector and vector form factors for the decay is determined independently (e.g., from a β-ν correlation measurement), a stand-alone β asymmetry measurement by itself cannot be used to place constraints on allowed values of δ and ζ. In facing such a scenario for ^{19}Ne β decay, one has to resort to the ratio

$$R = \left(\frac{\mathcal{F}t^{0^+\to 0^+}}{\mathcal{F}t^{^{19}\mathrm{Ne}}}\right), \tag{13}$$

where $\mathcal{F}t^{0^+\to 0^+} = 3072.27(72)$ s is the averaged $\mathcal{F}t$ value from $0^+ \to 0^+$ superallowed Fermi transitions [37].

If one permits the existence of RHCs ($x, y \neq 0$), then R can be expressed as [3]

$$R \simeq \left[\frac{a^2(1+x^2) + \left(\frac{f_A}{f_V}\right)c^2(1+y^2) + r_i}{2a^2(1+x^2)}\right], \tag{14}$$

[11]This analysis is valid only if the RH neutrinos are light enough not to kinematically suppress the decay.

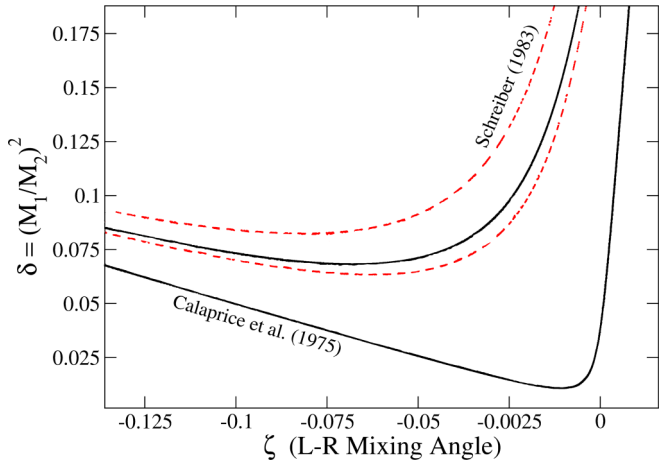

FIG. 8. A comparison of 90% CL constraints on δ and ζ set by two independent $A_\beta(0)$ measurements for ^{19}Ne decay (black solid line [1] and red dashed line [50]), together with the $\mathcal{F}t$ value obtained in this work. The allowed regions were generated assuming the manifest LR model.

where r_i are the small recoil-order corrections in Eq. (9). Therefore, it is imperative that *both* R and A_β are known with high precision and accuracy in order to place meaningful bounds on RHCs. On using the currently determined high-precision value for $\mathcal{F}t^{^{19}\mathrm{Ne}}$, we obtain $R = 1.785(1)$, which is three times more precise than known previously.

In Fig. 8 we show the 90% CL allowed region in the (δ, ζ) parameter space, obtained[12] from a simultaneous fit to R and the β asymmetry measured by Calaprice *et al.* [1]. Despite the fact that the measured dA_β/dE from the same experiment yielded a much larger slope than expected, we choose this value of $A_\beta(0)$ for the following reasons. First, it is the latest (and most precise) *published* β asymmetry measurement for ^{19}Ne decay. Second, together with the $\mathcal{F}t^{^{19}\mathrm{Ne}}$ value in Eq. (7), the other asymmetry measurements of Refs. [48–51] yield values for the V_{ud} matrix element (cf. Sec. V C) that are much smaller than expected. Consequently, together with the current Particle Data Group (PDG) recommended values [67,68] for V_{us} and V_{ub}, these results lead to significant violations of the CKM unitarity condition.[13] For the sake of comparison we also show in Fig. 8 the 90% CL bounds obtained using the most precise reported (unpublished) value of the β asymmetry parameter by Schreiber [50]. The ratio of the Gamow-Teller to Fermi form factors obtained from this measurement is in almost exact agreement with the independent determinations of Refs. [49,51] (cf. Fig. 7). Furthermore, the energy dependence dA_β/dE determined from Schreiber's experiment shows no indication of second-class currents and is also in excellent agreement with the later measurement by Jones [51]. However, despite this consistency, the quoted $A_\beta(0)$ value from

[12]We set $d = 0$ in this part of the analysis and the next subsection.

[13]The extracted values of V_{ud} from the results of Refs. [48,50,51] result in a violation of CKM unitarity by 5 standard deviations or more. The value obtained from the 1969 measurement [49] can also be ruled out as it disagrees with unitarity at the 99.6% CL.

this experiment shows a significantly large signal for RHCs, as apparent in Fig. 8. This should not be surprising, given the CKM unitarity violation mentioned previously. The best fit to these data disagrees with the standard model prediction for no RHCs ($\delta = \zeta = 0$) at the 6.4σ level. In contrast, the best fit using the result from Ref. [1] deviates from the standard model by only 1.7σ.

In light of the above, we conclude that the systematic effects that might have affected the A_β slope measurement in Ref. [1] did not significantly influence their extraction of the zero kinetic energy intercept value $A_\beta(0)$. All the other measured values for the β asymmetry (except the lowest-precision measurement from 1963) can be ruled out. There has been a recent effort [69] to reanalyze the data acquired by Ref. [51], by placing emphasis on positron backscattering and other systematic effects. The results from this reanalysis are expected to be published soon [70].

C. A determination of V_{ud}

It was implicit in the previous discussion that if one assumes conservation of the vector current, the $\mathcal{F}t$ value in Eq. (7) determines [7] the V_{ud} element of the CKM quark-mixing matrix. The expression to obtain V_{ud} is analogous to neutron decay, where

$$V_{ud} = \left[\frac{K}{\mathcal{F}t G_F^2}\frac{1}{\left(1+\Delta_R^V\right)\left(1+\frac{f_A}{f_V}\rho^2 + r_i\right)}\right]^{1/2}. \qquad (15)$$

Here $K/(\hbar c)^6 = 2\pi^3\hbar\ln 2/(m_e c^2)^5 = 8120.2776(9)\times 10^{-10}$ GeV^{-4} s [37], $G_F/(\hbar c)^3 = 1.1663787(6)\times 10^{-5}$ GeV^{-2} is the universal Fermi coupling constant [71], $\Delta_R^V = 2.361(38)\%$ is a nucleus independent electroweak radiative correction [72] and $\rho = c/a$. Needless to say, determining V_{ud} in this manner requires an independent correlation measurement to obtain the mixing ratio ρ. We obtain $\rho = -1.5995(45)$ from the $A_\beta(0)$ measurement of Ref. [1]. Using this value of ρ and the $\mathcal{F}t$ value determined in this work, we obtain $V_{ud} = 0.9707(22)$. This is in reasonable agreement with the high-precision value extracted from superallowed $0^+ \to 0^+$ Fermi transitions [37].

It should be noted that the radiative correction mentioned above was recently revaluated to be $\Delta_R^V = 2.467(22)\%$ [73] using dispersion relations together with neutrino-scattering data. However, incorporating this new result has an insignificant effect on our extracted value for V_{ud}, as the latter's uncertainty is dominated by the uncertainty contribution from $A_\beta(0)$.

D. Toward a better understanding of parity-violating *NN* interactions

The $J^\pi = (1/2^+; 1/2^-)$, $T = 1/2$ parity doublet in ^{19}F (shown in Fig. 1) plays an important role in elucidating both the isoscalar and isovector components of $\Delta S = 0$ parity nonconserving (PNC) hadronic weak interactions [11,74]. It is one of the few cases where the PNC *NN* interaction admixes the doublet states significantly, on account of the small energy spacing between the levels ($\Delta E = 110$ keV) and the absence of other nearby $J = 1/2$ states. This leads to an amplification of the parity-violating observable, namely the asymmetry of the 110-keV γ rays that would be emitted from a polarized ensemble of ^{19}F nuclei in the first excited $1/2^-$ state. The γ asymmetry has been measured independently by two groups, whose results are in excellent agreement with each other [10,75]. However, these experimental results are approximately three times smaller than shell-model predictions [8,9] that used the "best values" recommended by Desplanques, Donoghue, and Holstein [11,74,76] for the weakly interacting PNC meson-nucleon couplings.

It has been shown that the model dependence in extracting the weak *NN* amplitudes from the PNC observables can be largely minimized in such cases via measurements of the β-decay transition rates connecting the isobaric analog of one member of the doublet to the other [10]. Here it is the first-forbidden $1/2^+ \to 1/2^-$ transition in ^{19}Ne β^+ decay. In the $q^2 \to 0$ limit, the forbidden β-decay matrix element is dominated by the $\Delta J^\pi = 0^-$ axial-charge operator and is very similar to the isovector part of the parity mixing matrix element. Therefore, not only does the measured $1/2^+ \to 1/2^-$ ^{19}Ne β-decay rate offer a model-independent means to calculate the isovector PNC *NN* amplitudes, but also it allows a useful check of the wave functions that are used to analyze the parity mixing in ^{19}F. A previous analysis showed that the calculated decay rate was about 10 times larger than the measured values [31], presumably because of the omission of $5p$-$2h$ correlations in the shell-model wave functions. This would explain the factor-of-3 discrepancy between the measured and calculated values of the γ asymmetry mentioned previously, assuming that the isoscalar contribution of the parity-violating matrix element also scales similarly [10]. It has been suggested [10,31] that a large-basis shell-model calculation which includes $2\hbar\omega$ excitations would resolve this issue.

In light of the above and the recent development of state-of-the-art computational techniques [77–81] to extract elementary PNC amplitudes, we anticipate our high-precision measurement of the first-forbidden branch will be useful to constrain future calculations. Together with the high-precision values for the ^{19}Ne half-life and a weighted mean of the results in Table II, we obtain a first-forbidden transition rate of $\omega_{\rm expt} = 4.06(28)\times 10^{-6}$ s^{-1}. On further assuming an allowed spectrum shape[14] for the first forbidden transition [31] we determine its ft value to be $1.35(9)\times 10^7$ s. Our values are roughly two times more precise yet in agreement with previous measurements.

VI. CONCLUSIONS

We measured β-decay branches to excited states in ^{19}F for the first time using a radioactive ^{19}Ne beam. Unlike previous measurements that used (p, n) reactions on gas targets, our experiment was minimally affected by the source distribution and other associated systematic effects. We obtain high-precision values for the β transition rates that would be useful

[14] This is a reasonable approximation as the axial-charge operator is independent of the momentum transferred to the leptons [10,31].

for a variety of fundamental symmetry tests that involve ^{19}Ne and ^{19}F nuclei.

ACKNOWLEDGMENTS

We thank Ian Towner for calculating the statistical rate functions. We are also grateful to Alejandro García, Eric Adelberger, Wick Haxton, and Dan Melconian for fruitful discussions. This work was partially funded by the National Research Foundation (NRF) of South Africa and the Natural Sciences and Engineering Research Council of Canada (NSERC). P.Z.M. thanks the NRF funded MANUS/MATSCI program at UWC/UZ for financial support during the course of her M.Sc. TRIUMF receives federal funding via a contribution agreement through the National Research Council of Canada.

[1] F. P. Calaprice, S. J. Freedman, W. C. Mead, and H. C. Vantine, Phys. Rev. Lett. **35**, 1566 (1975).
[2] A. S. Carnoy, J. Deutsch, R. Prieels, N. Severijns, and P. A. Quin, J. Phys. G: Nucl. Part. Phys. **18**, 823 (1992).
[3] B. R. Holstein and S. B. Treiman, Phys. Rev. D **16**, 2369 (1977).
[4] B. R. Holstein, Phys. Rev. C **16**, 753 (1977).
[5] A. L. Hallin, F. P. Calaprice, D. W. MacArthur, L. E. Piilonen, M. B. Schneider, and D. F. Schreiber, Phys. Rev. Lett. **52**, 337 (1984).
[6] M. B. Schneider, F. P. Calaprice, A. L. Hallin, D. W. MacArthur, and D. F. Schreiber, Phys. Rev. Lett. **51**, 1239 (1983).
[7] O. Naviliat-Cuncic and N. Severijns, Phys. Rev. Lett. **102**, 142302 (2009).
[8] W. C. Haxton, B. F. Gibson, and E. M. Henley, Phys. Rev. Lett. **45**, 1677 (1980).
[9] B. A. Brown, W. A. Richter, and N. S. Godwin, Phys. Rev. Lett. **45**, 1681 (1980).
[10] E. G. Adelberger, M. M. Hindi, C. D. Hoyle, H. E. Swanson, R. D. Von Lintig, and W. C. Haxton, Phys. Rev. C **27**, 2833 (1983).
[11] E. G. Adelberger and W. C. Haxton, Ann. Rev. Nucl. Part. Sci. **35**, 501 (1985).
[12] A. B. Garnsworthy and P. E. Garrett, Hyperfine Interact. **225**, 121 (2014).
[13] P. E. Garrett *et al.*, J. Phys.: Conf. Series **639**, 012006 (2015).
[14] S. Triambak *et al.*, Phys. Rev. Lett. **109**, 042301 (2012).
[15] P. Finlay *et al.*, Phys. Rev. C **78**, 025502 (2008).
[16] K. G. Leach *et al.*, Phys. Rev. Lett. **100**, 192504 (2008).
[17] R. Dunlop *et al.*, Phys. Rev. C **88**, 045501 (2013).
[18] J. Sempau, E. Acosta, J. Baro, J. Fernández-Varea, and F. Salvat, Nucl. Instrum. Methods B **132**, 377 (1997).
[19] http://www.srim.org/.
[20] J. F. Ziegler, M. D. Ziegler, and J. P. Biersack, Nucl. Instrum. Methods B **268**, 1818 (2010).
[21] V. E. Iacob, J. C. Hardy, C. A. Gagliardi, J. Goodwin, N. Nica, H. I. Park, G. Tabacaru, L. Trache, R. E. Tribble, Y. Zhai, and I. S. Towner, Phys. Rev. C **74**, 015501 (2006).
[22] S. Baker and R. D. Cousins, Nucl. Instrum. Methods **221**, 437 (1984).
[23] P. Ujić *et al.*, Phys. Rev. Lett. **110**, 032501 (2013).
[24] C. Fontbonne *et al.*, Phys. Rev. C **96**, 065501 (2017).
[25] L. J. Broussard *et al.*, Phys. Rev. Lett. **112**, 212301 (2014).
[26] G. F. Grinyer *et al.*, Nucl. Instrum. Methods A **579**, 1005 (2007).
[27] P. Finlay, M.Sc. thesis, University of Guelph, 2007, https://www.physics.uoguelph.ca/Nucweb/theses/paulfinlay_62Ga_mscthesis.pdf.
[28] S. J. Freedman, R. M. Del Vecchio, and C. Callias, Phys. Rev. C **12**, 315 (1975).
[29] N. Severijns, M. Tandecki, T. Phalet, and I. S. Towner, Phys. Rev. C **78**, 055501 (2008).
[30] D. E. Alburger, Phys. Rev. C **13**, 2593 (1976).
[31] E. G. Adelberger, M. M. Hindi, C. D. Hoyle, H. E. Swanson, and R. D. Von Lintig, Phys. Rev. C **24**, 313 (1981).
[32] E. R. J. Saettler, F. P. Calaprice, A. L. Hallin, and M. M. Lowry, Phys. Rev. C **48**, 3069 (1993).
[33] R. B. Firestone *et al.* (eds.), in *Table of Isotopes*, 8th ed. (Wiley, New York, 1966).
[34] W. Bambynek *et al.*, Rev. Mod. Phys. **49**, 77 (1977).
[35] https://www-nds.iaea.org/amdc/.
[36] M. Wang, G. Audi, F. Kondev, W. Huang, S. Naimi, and X. Xu, Chin. Phys. C **41**, 030003 (2017).
[37] J. C. Hardy and I. S. Towner, Phys. Rev. C **91**, 025501 (2015).
[38] S. Triambak *et al.*, Phys. Rev. C **95**, 035501 (2017).
[39] L. Grenacs, Ann. Rev. Nucl. Part. Sci. **35**, 455 (1985).
[40] I. S. Towner (private communication) (2018).
[41] B. R. Holstein, Rev. Mod. Phys. **46**, 789 (1974).
[42] V. Cirigliano, S. Gardner, and B. R. Holstein, Prog. Part. Nucl. Phys. **71**, 93 (2013).
[43] S. Weinberg, Phys. Rev. **112**, 1375 (1958).
[44] B. R. Holstein and S. B. Treiman, Phys. Rev. C **3**, 1921 (1971).
[45] B. R. Holstein, Phys. Rev. C **9**, 1742 (1974).
[46] R. P. Feynman and M. Gell-Mann, Phys. Rev. **109**, 193 (1958).
[47] E. D. Commins and D. A. Dobson, Phys. Rev. Lett. **10**, 347 (1963).
[48] F. P. Calaprice, E. D. Commins, H. M. Gibbs, G. L. Wick, and D. A. Dobson, Phys. Rev. Lett. **18**, 918 (1967).
[49] F. P. Calaprice, E. D. Commins, H. M. Gibbs, G. L. Wick, and D. A. Dobson, Phys. Rev. **184**, 1117 (1969).
[50] D. F. Schreiber, Ph.D. thesis, Princeton University, 1983.
[51] G. L. Jones, Ph.D. thesis, Princeton University, 1996.
[52] R. E. Tribble, D. P. May, and D. M. Tanner, Phys. Rev. C **23**, 2245 (1981).
[53] R. E. Tribble and D. P. May, Phys. Rev. C **18**, 2704 (1978).
[54] K. Minamisono *et al.*, Phys. Rev. C **84**, 055501 (2011).
[55] K. Minamisono, K. Matsuta, T. Minamisono, T. Yamaguchi, T. Sumikama, T. Nagatomo, M. Ogura, T. Iwakoshi, M. Fukuda, M. Mihara, K. Koshigiri, and M. Morita, Phys. Rev. C **65**, 015501 (2001).
[56] J. C. Pati and A. Salam, Phys. Rev. D **10**, 275 (1974).
[57] G. Senjanović and R. N. Mohapatra, Phys. Rev. D **12**, 1502 (1975).
[58] N. Shaban and W. Stirling, Phys. Lett. B **291**, 281 (1992).
[59] P. Herczeg, Prog. Part. Nucl. Phys. **46**, 413 (2001).
[60] M. A. B. Bég, R. V. Budny, R. Mohapatra, and A. Sirlin, Phys. Rev. Lett. **38**, 1252 (1977).
[61] P. Langacker and S. U. Sankar, Phys. Rev. D **40**, 1569 (1989).

[62] R. N. Mohapatra and G. Senjanović, Phys. Rev. Lett. **44**, 912 (1980).
[63] G. Branco, J.-M. Frère, and J.-M. Gérard, Nucl. Phys. B **221**, 317 (1983).
[64] A.-S. Carnoy, J. Deutsch, and B. R. Holstein, Phys. Rev. D **38**, 1636 (1988).
[65] O. Naviliat-Cuncic, T. A. Girard, J. Deutsch, and N. Severijns, J. Phys. G: Nucl. Part. Phys. **17**, 919 (1991).
[66] B. Fenker, A. Gorelov, D. Melconian, J. A. Behr, M. Anholm, D. Ashery, R. S. Behling, I. Cohen, I. Craiciu, G. Gwinner, J. McNeil, M. Mehlman, K. Olchanski, P. D. Shidling, S. Smale, and C. L. Warner, Phys. Rev. Lett. **120**, 062502 (2018).
[67] http://pdg.lbl.gov/.
[68] M. Tanabashi *et al.* (Particle Data Group), Phys. Rev. D **98**, 030001 (2018).
[69] D. Combs, F. Calaprice, G. Jones, and A. Young, in *APS Division of Nuclear Physics Meeting Abstracts* (American Physical Society, 2016), p. KG.008.
[70] A. R. Young (private communication) (2018).
[71] V. Tishchenko *et al.* (MuLan Collaboration), Phys. Rev. D **87**, 052003 (2013).
[72] W. J. Marciano and A. Sirlin, Phys. Rev. Lett. **96**, 032002 (2006).
[73] C.-Y. Seng, M. Gorchtein, H. H. Patel, and M. J. Ramsey-Musolf, Phys. Rev. Lett. **121**, 241804 (2018).
[74] W. Haeberli and B. R. Holstein, in *Symmetries and Fundamental Interactions in Nuclei*, edited by W. Haxton and E. Henley (World Scientific, Singapore, 1995), p. 17.
[75] K. Elsener, W. Grüebler, V. König, P. A. Schmelzbach, J. Ulbricht, D. Singy, C. Forstner, W. Z. Zhang, and B. Vuaridel, Phys. Rev. Lett. **52**, 1476 (1984).
[76] B. Desplanques, J. F. Donoghue, and B. R. Holstein, Ann. Phys. **124**, 449 (1980).
[77] J. Wasem, Phys. Rev. C **85**, 022501(R) (2012).
[78] D. R. Phillips, D. Samart, and C. Schat, Phys. Rev. Lett. **114**, 062301 (2015).
[79] M. R. Schindler, R. P. Springer, and J. Vanasse, Phys. Rev. C **93**, 025502 (2016).
[80] W. C. Haxton and B. R. Holstein, Prog. Part. Nucl. Phys. **71**, 185 (2013).
[81] S. Gardner, W. C. Haxton, and B. R. Holstein, Ann. Rev. Nucl. Part. Sci. **67**, 69 (2017).